Assimilation of T-TREC-Retrieved Winds from Single-Doppler Radar with an Ensemble Kalman Filter for the Forecast of Typhoon Jangmi (2008)

MINGJUN WANG

Key Laboratory for Mesoscale Severe Weather/MOE and School of Atmospheric Science, Nanjing University, Nanjing, China, and Center for Analysis and Prediction of Storms, University of Oklahoma, Norman, Oklahoma

MING XUE

Key Laboratory for Mesoscale Severe Weather/MOE and School of Atmospheric Science, Nanjing University, Nanjing, China, and Center for Analysis and Prediction of Storms and School of Meteorology, University of Oklahoma, Norman, Oklahoma

KUN ZHAO

Key Laboratory for Mesoscale Severe Weather/MOE and School of Atmospheric Science, Nanjing University, Nanjing, China

JILI DONG

Center for Analysis and Prediction of Storms, University of Oklahoma, Norman, Oklahoma

(Manuscript received and in final form 7 December 2013)

ABSTRACT

A tropical cyclone (TC) circulation Tracking Radar Echo by Correlation technique (T-TREC) developed recently is applied to derive horizontal winds from single Doppler radar reflectivity Z data (combined with radial velocity V_r data when available). The typically much longer maximum range of Z observations compared to V_r data allows for much larger spatial coverage of the T-TREC-retrieved winds (V_{TREC}) when a TC first enters the maximum range of a coastal radar. Retrieved using data from more than one scan volume, the T-TREC winds also contain valuable cross-beam wind information. The V_{TREC} or V_r data at 30-min intervals are assimilated into the Advanced Regional Prediction System (ARPS) model at 3-km grid spacing using an ensemble Kalman filter, over a 2-h window shortly after Typhoon Jangmi (2008) entered the V_r coverage area of an operational weather radar of Taiwan. The assimilation of V_{TREC} data produces analyses of the typhoon structure and intensity that more closely match observations than analyses produced using V_r data or the reference Global Forecast System (GFS) analysis. Subsequent 28-h forecasts of intensity, track, structure, and precipitation are also improved by assimilating V_{TREC} data. Further sensitivity experiments show that assimilation of V_{TREC} data can build up a reasonably strong vortex in 1 h, while a longer assimilation period is required to spin up the vortex when assimilating V_r. Although the difference between assimilating V_{TREC} and V_r is smaller when the assimilation window is longer, the improvement from assimilating V_{TREC} is still evident. Assimilating Z data in addition to V_r or V_{TREC} results in little further improvement.

1. Introduction

Doppler weather radar is an important instrument for observing landfalling tropical cyclones (TCs) at high spatial and temporal resolutions. In recent years, radial velocity V_r and/or radar reflectivity Z data from ground-based coastal Doppler radars have been assimilated into high-resolution numerical weather prediction (NWP) models to improve TC forecasts, primarily using a three-dimensional variational data assimilation (DA) (3DVAR) system (e.g., Xiao et al. 2007; Zhao and Jin 2008; Zhao and Xue 2009; Zhao et al. 2012a,b) or an ensemble Kalman filter (EnKF; e.g., Zhang et al. 2009; Dong and Xue 2013, hereafter DX13; Xue and Dong 2013). Compared with 3DVAR using static background error covariance, the EnKF can estimate flow-dependent background error covariance through an ensemble of

Corresponding author address: Dr. Ming Xue, Center for Analysis and Prediction of Storms, University of Oklahoma, 120 David Boren Blvd., Norman, OK 73072.
E-mail: mxue@ou.edu

DOI: 10.1175/MWR-D-13-00387.1

forecasts and theoretically has significant advantages for TC analysis (Zhang et al. 2009; Hamill et al. 2011).

For typical S band operational weather surveillance radars, including the Weather Surveillance Radar-1988 Doppler (WSR-88D) of the United States and the China New Generation Radar-1998 Doppler (CINRAD-98D) of China, the maximum range of V_r measurements is 230 km, limiting radar coverage of TCs when they are located far from the coast. The maximum range of Z measurements of these radar systems extends about twice as far, providing potentially very useful information before the core region of the TC moves into the V_r coverage area. The assimilation of Z has produced positive impacts on hurricane analysis and forecasting within 3DVAR frameworks (Xiao et al. 2007; Zhao and Jin 2008; Zhao and Xue 2009), but V_r data generally have larger impacts than Z data for TC initialization (Zhao and Jin 2008; Zhao and Xue 2009; DX13).

Apart from providing direct information on precipitation, reflectivity has been used to derive wind fields within TCs using the Tracking Radar Echo by Correlation (TREC) method, assuming that reflectivity changes between two successive radar volume scans are mainly caused by advection (Tuttle and Gall 1999). Harasti et al. (2004) modified the TREC technique for the real-time wind analysis of TCs at different altitudes. Recently, Wang et al. (2011) developed the TC circulation TREC (T-TREC) technique by extending TREC to polar coordinates (centered on the TC) and constraining the local echo tracking region using the vortex rotation rate estimated from available V_r data. T-TREC has been used for diagnosing TC circulations in realtime at the China Meteorological Administration (CMA).

The V_r only contains the along-beam component of the wind field, thus when assimilating V_r from a single radar the cross-beam components of winds are often retrieved poorly (Zhao et al. 2012a,b). The full three-dimensional wind field retrieved from a single Doppler radar can, however, be valuable for TC initialization. Zhao et al. (2012a) investigated the impact of assimilating ground-based velocity track display (GBVTD)-retrieved winds from a single Doppler radar, and found that doing so resulted in an improved analysis and forecast of a typhoon compared to an analysis obtained by assimilating V_r data directly. The cross-beam wind component and more-complete spatial coverage provided by GBVTD-retrieved winds in the TC inner core region were the primary reasons for the better performance of GBVTD-retrieved winds compared to V_r. The drawback with GBVTD retrievals is that the data do not contain asymmetric wind components beyond wavenumber 3; therefore, more detailed asymmetric structures presented in V_r data may be lost. Retrieved from two time levels of three-dimensional Z observations, the T-TREC winds (V_{TREC}) are not subject to such limitations; they contain retrieved cross-beam winds and generally have a much wider data coverage area than V_r (because of the typically longer range of Z compared to V_r for operational radars) and GBVTD-retrieved winds (which are derived from V_r observations). For these reasons, V_{TREC} data have the potential to improve the analysis and initialization of the inner core structures of TCs approaching landfall.

Recently, Li et al. (2013) explored the assimilation of V_{TREC} winds using the Weather Research and Forecasting Model (WRF) 3DVAR system (Barker et al. 2004; Xiao et al. 2005) for the analysis and forecast of Typhoon Meranti (2010) before it made landfall at Fujian Province at the southeast coast of China. They assimilated V_{TREC} or V_r data from a single coastal radar at a single time approximately 8, 6, 4, or 2 h prior to landfall. Their results indicate that assimilation of V_{TREC} data leads to better analysis of the structure and intensity of the typhoon than directly can be obtained assimilating V_r data. The subsequent forecasts for the typhoon track, intensity, structure, and precipitation are also improved, although the differences become smaller for the latter analysis times when V_r data coverage improves as the typhoon approaches the radar. The larger spatial coverage of V_{TREC} data and the cross-beam information it contains are believed to be the primary reasons for the superior performance of V_{TREC} over V_r data.

Parallel to the effort of Li et al. (2013), this study examines the impacts of cycled assimilation of V_{TREC} data on the analysis and forecasting of Typhoon Jangmi (2008), using an ensemble Kalman filter (EnKF) at a convection-permitting resolution. Typhoon Jangmi made landfall on the east coast of Taiwan on 28 September 2008. Before and during its landfall, the TC inner core was observed by an operational S band Doppler radar located at Hualian, Taiwan, from 0000 UTC 28 September to 0000 UTC 29 September. In this study, the retrieved V_{TREC} data are assimilated using EnKF through 30-min assimilation cycles for 1–3 h prior to Jangmi entered the observation range of Hualian radar. The impacts of assimilating V_{TREC} data on the track, intensity, structure, and precipitation forecasts are examined, and the analyses thus obtained are compared with analyses obtained by assimilating V_r data directly. The impacts of assimilating reflectivity data in addition to V_{TREC} or V_r data are also examined.

The rest of this paper is organized as follows. Section 2 describes the forecast model, radar data, and experimental design. The results of the first set of experiments that assimilate radar data for 2 h are first presented in section 3, together with discussions on the impacts of the

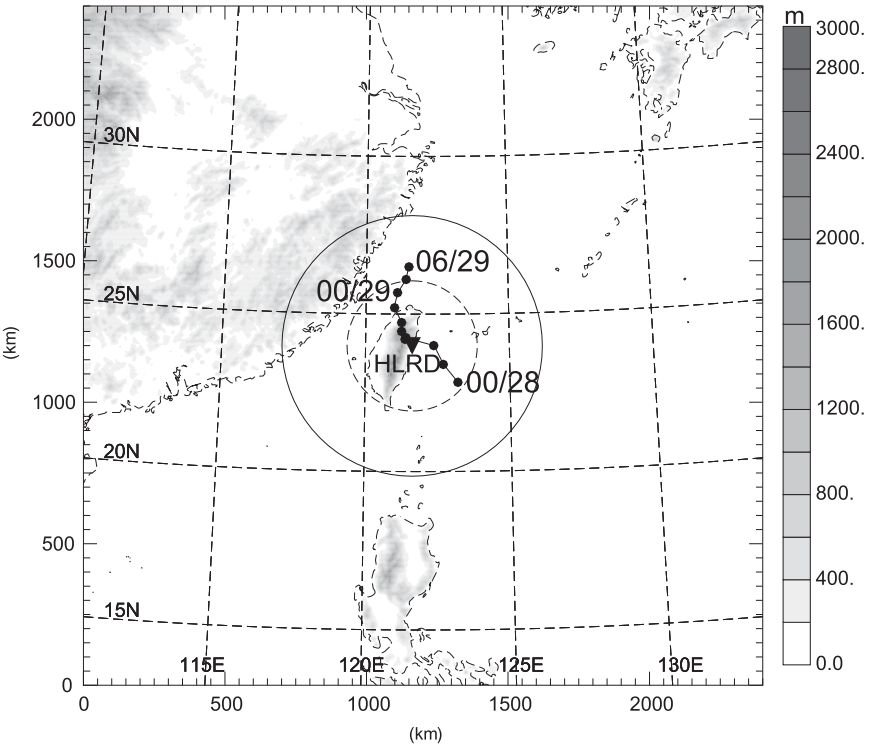

FIG. 1. The physical domain of the numerical simulation, with the average best track (ABT, see section 2) locations plotted every 3 h from 0000 UTC 28 Sep to 0600 UTC 29 Sep 2008 (marked by black dots). The triangle denotes the position of Hualian radar (HLRD), and its observation ranges for radial velocity and radar reflectivity are denoted by dashed and solid circles, respectively. The gray shading indicates terrain height (m).

radar data on the analyses and forecasts. Section 4 presents the results of sensitivity experiments that examine the impacts of assimilation window length (of 1 or 3 h) and reflectivity assimilation. Conclusions and discussion are presented in section 5.

2. Model, radar data, and experimental design

a. The prediction model

The Advanced Regional Prediction System (ARPS; Xue et al. 2000, 2001) version 5.3 is used as the prediction model. The physical domain is 2400 × 2400 × 25 km^3 and has a 3-km horizontal grid spacing (Fig. 1). A stretched vertical grid is used; the mean vertical grid spacing is 500 m, with a minimum vertical spacing of 20 m near the surface. Full model physics are used, including the Lin ice microphysics scheme (Lin et al. 1983), Goddard Space Flight Center (GSFC) longwave and shortwave radiation parameterization, a two-layer force-restore soil-vegetation model (Ren and Xue 2004), 1.5-order turbulent kinetic energy (TKE)-based subgrid-scale turbulence (Deardorff 1980), and PBL parameterization (Xue et al. 1996). For this study in particular, a new surface flux parameterization scheme for the ocean surface based on Makin (2005) is implemented into the ARPS and used in this study. Different from the original scheme in the ARPS, based on (Anderson 1993) and having the drag coefficient linearly increasing with the surface wind speed (see, Xue et al. 1995), the new scheme reduces the drag coefficient for wind speeds exceeding 33 m s^{-1} based on field measurement data (Powell et al. 2003). This new scheme is found to allow for the prediction of larger surface wind speeds than the original formulation, though the overall intensity of the analyzed and predicted typhoon is not substantially changed in our experiments. The initial analysis background and the lateral boundary conditions (LBCs) are obtained from the National Centers for Environmental Prediction (NCEP) operational Global Forecast System (GFS).

b. Radar data processing and quality control

The V_r and Z data from Hualian radar on the east coast of Taiwan (HLRD, Fig. 1) are first manually edited, including velocity dealiasing and ground clutter removal. To retrieve V_{TREC}, Z, and V_r data are first interpolated to

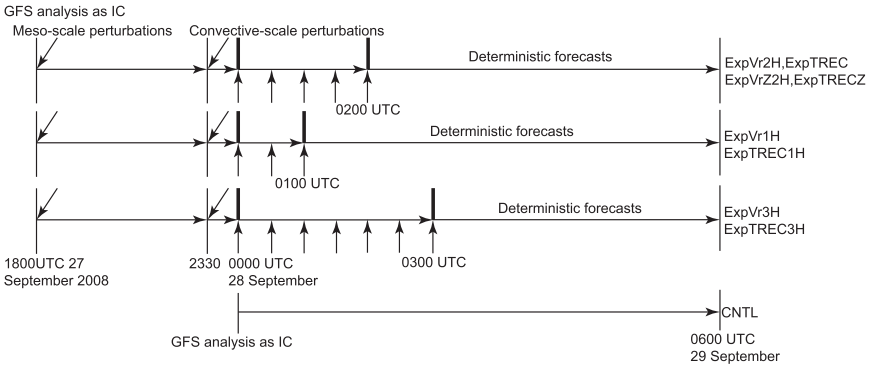

FIG. 2. EnKF data assimilation and forecast flowcharts for all experiments. The vertical arrows denote assimilation of radar data and the slanted arrows at 1800 and 2330 UTC denote the addition of two sets of perturbations to generate the ensemble.

a grid with 1-km grid spacing in both horizontal and vertical; the retrieval is performed within a 300-km radius of the TC center at each level from 1 to 8 km. To keep the retrieved V_{TREC} data mostly independent, the retrieval was performed on a grid with horizontal grid spacing of 10 km, and the retrieved data are directly assimilated. More details on the T-TREC technique can be found in Wang et al. (2011). When assimilating V_r data for comparison, the data are interpolated in the horizontal to the ARPS model columns but kept on radar elevation levels in the vertical.

The V_{TREC} data at 3 km above the surface at 0000 UTC 28 September 2008 are shown along with the observed Z (in Fig. 3a), along with observed V_r (in Fig. 3b), and along with the V_r simulated from V_{TREC} data (by projecting to the radar radial directions; in Fig. 3c). Observed V_r is limited to a maximum range of 230 km, resulting in an incomplete velocity dipole pattern with areas of missing data (Fig. 3b). T-TREC retrieves the cross-beam velocity and fills the V_r data voids quite effectively (Fig. 3a). The simulated V_r shows a similar pattern as the observed V_r within the 230-km radius, suggesting that V_{TREC} (including the cross-beam component) estimates are reasonably accurate both within and outside of the V_r coverage area (Fig. 3c). The root-mean-square error of simulated V_r against the observed V_r is about 3.8 m s^{-1} during the 3-h DA window (see Fig. 2), which is consistent with the corresponding error statistics of less than 4 m s^{-1} from data samples examined in Wang et al. (2011). During EnKF DA, observation error standard deviations for V_r and V_{TREC} are specified as 2 and 5 m s^{-1}, respectively, guided by the error statistics of our data samples.

c. *EnKF experiments and settings*

A baseline control forecast (CNTL) without radar DA is run from 0000 UTC 28 September to 0600 UTC 29 September, initialized from the NCEP operational GFS analysis (Table 1). Following DX13, an initial forecast ensemble is generated by adding mesoscale perturbations at 1800 UTC 27 September and convective perturbations at 2330 UTC, 30 min before the first radar DA (see Fig. 2), giving a 6-h ensemble spinup period prior to DA. For additional details about the mesoscale and convective perturbations used, we refer the reader to DX13.

All DA experiments start from 0000 UTC 28 September and use 30-min assimilation cycles. For the first set of two DA experiments, ExpTREC2H and ExpVr2H, V_{TREC} and V_r data are assimilated within a 2-h window (Table 1; Fig. 2). This specific DA period is chosen because it is a period during which the main circulation of Jangmi was fully covered by Z data but not by V_r data (Fig. 3). The assimilation period is relatively short in order to maximize the forecast lead time prior to landfall of the typhoon; studies have also shown that it is usually the first few assimilation cycles for radar data that have the largest impact on TC initialization (DX13; Li et al. 2012). To further examine the impact of the DA window on the analysis and forecast, two additional pairs of experiments, ExpVr1H (ExpVr3H) and ExpTREC1H (ExpTREC3H) are run. These experiments are the same as ExpVr2H

TABLE 1. List of data assimilation and control experiments.

Expt	Obs assimilated	Assimilation window (h)
CNTL	No radar DA	—
ExpVr2H	V_r	2
ExpTREC2H	V_{TREC}	2
ExpVr1H	V_r	1
ExpTREC1H	V_{TREC}	1
ExpVr3H	V_r	3
ExpTREC3H	V_{TREC}	3
ExpVrZ2H	$V_r + Z$	2
ExpTRECZ2H	$V_{\mathrm{TREC}} + Z$	2

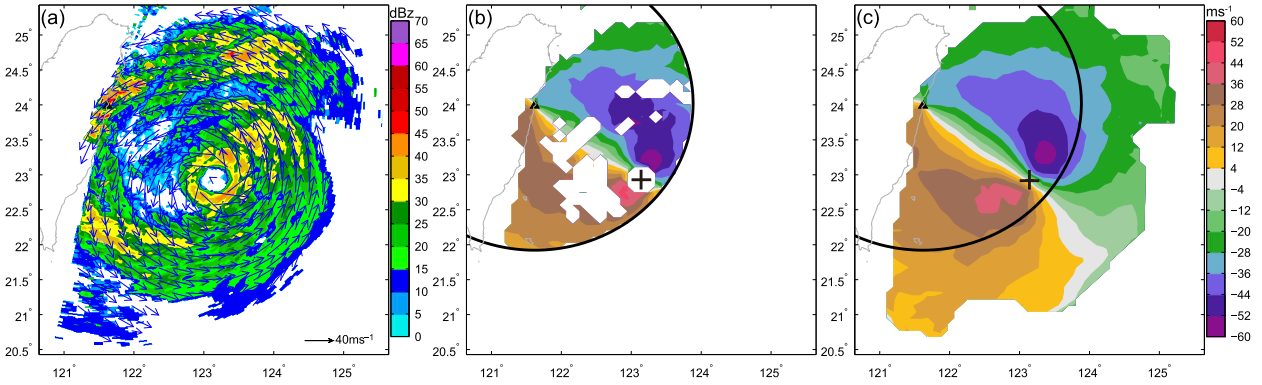

FIG. 3. The T-TREC analysis at 3 km above the surface at 0000 UTC 28 Sep 2008. (a) T-TREC-retrieved wind vectors overlaid with the observed reflectivity (color shaded, dBZ), (b) the observed Doppler radial velocity from HLRD, and (c) the radial velocity calculated from the T-TREC-retrieved winds (see section 2). The solid arcs indicate the maximum range of radial velocity data: 230 km from the radar. The plus symbol (+) denotes the center of the vortex, determined from radar reflectivity.

and ExpTREC2H except that they perform data assimilation for a period of 1 (3) h starting at the same time (Table 1; Fig. 2). In another pair of experiments, ExpVrZ2H and ExpTRECZ2H, radar reflectivity observations are assimilated in addition to V_r or V_{TREC} within a 2-h window. At the end of the assimilation window of each experiment, a deterministic forecast is launched and run until 0600 UTC 29 September. The workflows of the DA experiments are illustrated in Fig. 2.

Considering the different observation densities (Zhang et al. 2009; Torn 2010), covariance localization radii of 50 (10) km in the horizontal and 4 km in the vertical are used when assimilating V_{TREC} (V_r) data. A posterior relaxation to prior adaptive covariance inflation (Whitaker and Hamill 2012) with $\alpha = 0.9$ is applied at those model grid points directly influenced by observations to help maintain the ensemble spread. In addition to experience obtained from DX13, sensitivity experiments were performed to arrive at the current optimized DA configuration.

The deterministic forecasts are verified against the best track data and precipitation observations. During the verification period, which extends from 0000 UTC 28 September to 0600 UTC 29 September, best track data from the Japan Meteorological Agency (JMA), Taiwan Central Weather Bureau (CWB), and the Joint Typhoon Warning Center (JTWC) have significant differences; standard deviations of track, minimum sea level pressure (MSLP), and maximum surface wind (MSW) are as large as 31 km, 10 hPa, and 8 m s^{-1}, respectively. Uncertainties in best track estimates are also well recognized in recent studies (Torn and Snyder 2012; Landsea and Franklin 2013). In this study, average best track (ABT) data from these three operational centers is used for verification.

3. EnKF analyses and deterministic forecasts

a. *EnKF analyses of typhoon circulations and structures*

The horizontal winds at 3 km above the surface after the first EnKF analysis at 0000 UTC are shown in Figs. 4b,c for ExpVr2H and ExpTREC2H, together with the horizontal winds in the initial condition of CNTL, which are interpolated from GFS analysis valid at the same time (Fig. 4a). The vortex in the GFS analysis is too broad, with a radius of maximum wind (RMW) in excess of 100 km (Fig. 4a). In ExpVr2H, the RMW is only about 30 km, with the strongest winds found northeast and southwest of the eye (Fig. 4b). These strong winds are mostly in the radial direction of the HLRD radar, suggesting that the cross-beam wind component is underestimated in ExpVr2H. The inability of EnKF to accurately analyze the cross-beam wind component from single-Doppler radial velocity data was also noted in DX13; suspected causes include relatively poor quality of the background error covariance derived from ensemble forecasts of typhoons that are too weak, and possible prediction model error. More investigation of this problem is warranted in future studies, but such investigation is beyond the scope of the current study.

In ExpTREC2H, the vortex is much stronger than in ExpVr2H with a more continuous azimuthal circulation. The wind field does exhibit a prominent wavenumber-1 asymmetry structure, with the maximum of 45 m s^{-1} located in the northeastern quadrant (Fig. 4c), collocated with a region of strong convection observed by HLRD (Fig. 3a).

Figures 4d–f show the sea level pressure (SLP) and surface wind speed of the CNTL forecast and the final EnKF analyses of ExpVr2H and ExpTREC2H at 0200 UTC.

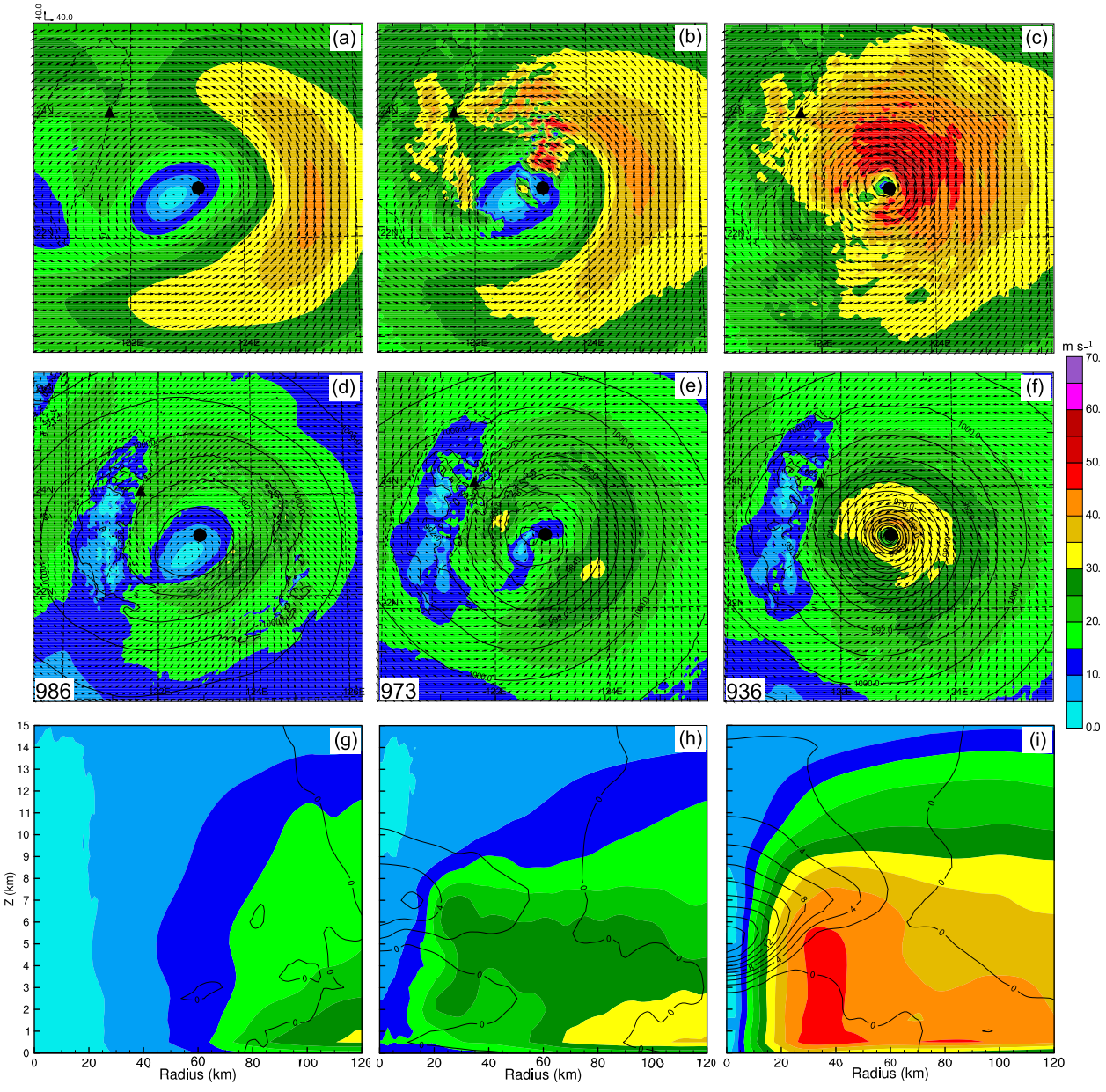

FIG. 4. (top) Horizontal wind vectors and speed (color shaded, $m\,s^{-1}$) at 3-km height and 0000 UTC from (a) the GFS analysis and analyses of (b) ExpVr2H and (c) ExpTREC2H. (middle) The SLP (contours) and surface wind speed (color shaded, $m\,s^{-1}$) at 0200 UTC in (d) CNTL, (e) ExpVr2H, and (f) ExpTREC2H. MSLP is shown at the bottom-left corner of each figure. (bottom) Azimuthally averaged tangential wind (color shaded) and temperature anomaly (contours with intervals of 2 K) at 0200 UTC for (g) CNTL, (h) ExpVr2H, and (i) ExpTREC2H. The black dot in the panels denotes the observed typhoon center, and the black triangles denote the location of RCHL.

The simulated vortex in CNTL has a MSLP of 986 hPa, much higher than the ABT value of 920 hPa (Fig. 4d). The MSLP of ExpVr2H is at 973 hPa while ExpTREC2H has the lowest value at 936 hPa, only 16 hPa above the ABT estimate. The circulation around the eyewall in ExpTREC2H is stronger than in both CNTL and ExpVr2H, with an annulus of wind speeds exceeding $30\,m\,s^{-1}$ around the center. ExpTREC2H also has the smallest position error (approximately 5 km).

To examine the vertical structure of the analyzed vortices, the azimuthally averaged tangential wind and temperature anomaly are presented in Figs. 4g–i. The temperature anomaly is defined as the deviation from the horizontal average within a 180-km radius (Liu et al.

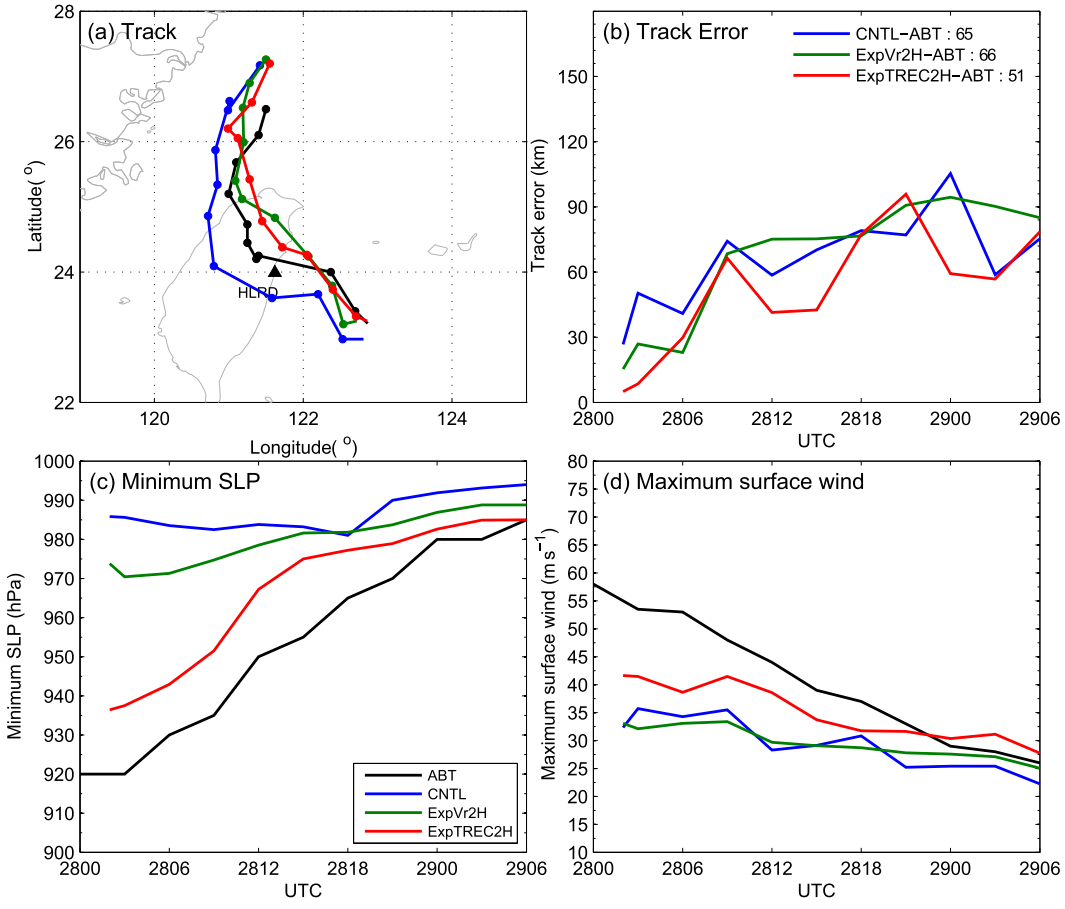

FIG. 5. The predicted (a) track, (b) track error, (c) MSLP, and (d) maximum surface wind speed from 0200 UTC 28 Sep to 0600 UTC 29 Sep 2008 for selected experiments, along with the average best track (ABT, see section 2). The dots in (a) denote the center locations every 3 h starting from 0300 UTC 28 Sep. The ABT at 0200 UTC 28 Sep is linearly interpolated from 0000 and 0300 UTC. The numbers in the legend of (b) denote the mean track errors over the 28-h forecast against the ABT.

1999). The vortex circulations of CNTL (Fig. 4g) and ExpVr2H (Fig. 4h) are weak and broad. ExpTREC2H (Fig. 4i) has a much tighter, stronger, and deeper vortex, with a RMW of only 30 km and a 30 m s^{-1} wind speed contour that extends as high as 8 km above the surface. The maximum temperature anomaly in ExpTREC2H is approximately 14 K at 6 km above the surface in the eye of the typhoon, suggesting a much stronger warm core than in either CNTL or ExpVr2H. Although the vertical structure cannot be directly verified by observation, the warm core structure is consistent with recent observation and simulation studies (Halverson et al. 2006; Stern and Nolan 2012) in terms of general warm core structure. The V_{TREC} data build a stronger vortex than V_r data due to the much more complete vortex circulation within the V_{TREC} data.

b. *Impacts on track and intensity predictions*

The predicted typhoon tracks, track errors, MSLPs, and MSWs from CNTL, ExpVr2H, and ExpTREC2H are plotted along with the ABT in Fig. 5. From 0200 UTC 28 September to 0600 UTC 29 September, Jangmi moved first to the northwest, then turned westward toward Taiwan. The track turned northwestward soon after landfall, then turned north-northeastward after the center passed over Taiwan (Fig. 5a). All three turns occur in the forecast of ExpTREC2H at locations close to those indicated in the ABT data, except for the final turn, which is substantially delayed. The track forecast of ExpTREC2H has a mean error of 51 km (Fig. 5b). The track of CNTL has the most westward bias, with a mean track error of approximately 65 km. ExpVr2H has the most northward track bias early on and lacks the initial westward and northwestward turns, resulting in a mean track error of about 66 km (Fig. 5b). Overall, ExpTREC2H has the smallest track error.

The MSLPs and MSWs from all three experiments are plotted along with those of the ABT in Figs. 5c and 5d, respectively. Starting from a relatively weak vortex with

a MSLP of 986 hPa, the typhoon intensity in CNTL does not change much during the forecast period, resulting in a mean MSLP error of 28 hPa and an error as large as 65 hPa at the initial condition time (0200 UTC). The intensity forecast is somewhat improved in ExpVr2H, but the mean MSLP error is still as large as 22 hPa during the forecast period and the initial error is around 53 hPa. In comparison, ExpTREC2H has a much smaller mean MSLP forecast error of about 11 hPa, and an initial error of only about 16 hPa; starting from a much lower initial MSLP, ExpTREC2H captures well the weakening of the typhoon as it makes landfall around 0800 UTC (Fig. 5c). Consistent with the much improved MSLP, the analyzed and predicted MSW in ExpTREC2H also show clear improvement compared to the other experiments (Fig. 5d). The initial MSW at 0200 UTC in ExpTREC2H is about 43 m s^{-1}, about 10 m s^{-1} higher than in ExpVr2H and CNTL; this difference is maintained for about 12 h. ExpTREC2H captures the weakening phase of the typhoon quite well. These results again show clear benefit of assimilating V_{TREC} data, even though there is still some intensity error (weak bias) in the final analysis of this very intense typhoon.

c. *Impacts on the forecast of typhoon structure*

To examine the impacts of V_{TREC} and V_r assimilation on Jangmi's structure in the forecast, the predicted composite reflectivity (column maximum) and horizontal wind vectors at 3-km height are presented in Fig. 6 for all three experiments, together with the observed composite reflectivity. At 0500 UTC, Jangmi has a rather compact eye with heavy precipitation in the southern and eastern quadrants of the vortex. The simulated typhoon in CNTL has a broad, elliptical eyewall with overly intense reflectivity (Fig. 6d). The eye in ExpVr2H is tighter and more circular, but still too large (Fig. 6g). The forecast typhoon in ExpTREC2H, which features the strongest predicted intensity, has a tighter vortex with a smaller eye (Fig. 6j) than that of ExpVr2H, and even contains some inner-core rainbands that appear to match radar observations (Fig. 6a). Similar to observations, precipitation in ExpTREC2H is most widespread in the southern and eastern quadrants of the storm.

In the 9-h forecast (after Jangmi has made landfall), the eye of the typhoon has filled in with precipitation, and the strongest echo (>35 dBZ) regions are located primarily over Taiwan (Fig. 6b). The inner-core precipitation over land is disrupted in CNTL, with an overly broad outer spiral rainband over the ocean (Fig. 6e). ExpVr2H (Fig. 6h) has a tight vortex over land and disorganized precipitation bands, while ExpTREC2H features the tightest vortex and inner rainbands located over Taiwan (Fig. 6k), including a north–south heavy precipitation band [due to interaction with the Central Mountain Range (CMR)] located farther east than in the observations (Fig. 6b). At 1700 UTC, the observed precipitation is highly asymmetric, and the strongest echoes are mostly located over southern Taiwan along the CMR (Fig. 6c). In all experiments, reflectivity patterns over land (Figs. 6f,i,l) agree well with the observations because of the interactions with the mountain range. In general, the rainbands in ExpTREC2H are closer to the typhoon center, resulting in better agreement with the observations than in CNTL and ExpVr2H, whose precipitation distributions are too broad. In summary, the assimilation of V_{TREC} or V_r data improves the predicted structure of Jangmi, and the best agreement with observations in terms of the predicted rainband structures and precipitation distributions occurs in ExpTREC2H.

d. *Precipitation forecasts*

The 12-h accumulated precipitation and the corresponding equitable threat scores (ETS) valid at 1400 UTC 28 September from all experiments are plotted in Fig. 7 together with the precipitation observations. The observed rainfall is obtained from quantitative precipitation estimation and segregation using multiple sensor (QPESUMS; Gourley et al. 2002) system data provided by the CWB of Taiwan. Prominent in the data is a strong precipitation band along the CMR (Fig. 7a). Two precipitation maxima are located over north and central Taiwan. These maxima are significantly underpredicted in ExpVr2H and CNTL (Figs. 7b,c), but better captured in ExpTREC2H, with the greatest improvement occurring for the northern maximum (Fig. 7d). ExpTREC2H also produces the highest ETSs (0.47, 0.41, and 0.35) for thresholds of 40, 80, and 120 mm, respectively. In summary, ExpTREC2H produces the best precipitation forecast both in terms of distribution and magnitude; these relatively good predictions can be attributed to the accuracy of track, intensity, and structure forecasts of the typhoon.

4. Sensitivity experiments

The experiments presented earlier used a 2-h-long assimilation window with 30-min DA cycles. To determine whether the conclusions regarding the relative impacts of T-TREC versus V_r data still hold when data are assimilated at different window lengths, two additional pairs of experiments are performed using 1- and 3-h assimilation windows. Another question one may ask is the following: When radar reflectivity data are also assimilated, does the relative impact of V_{TREC} and V_r

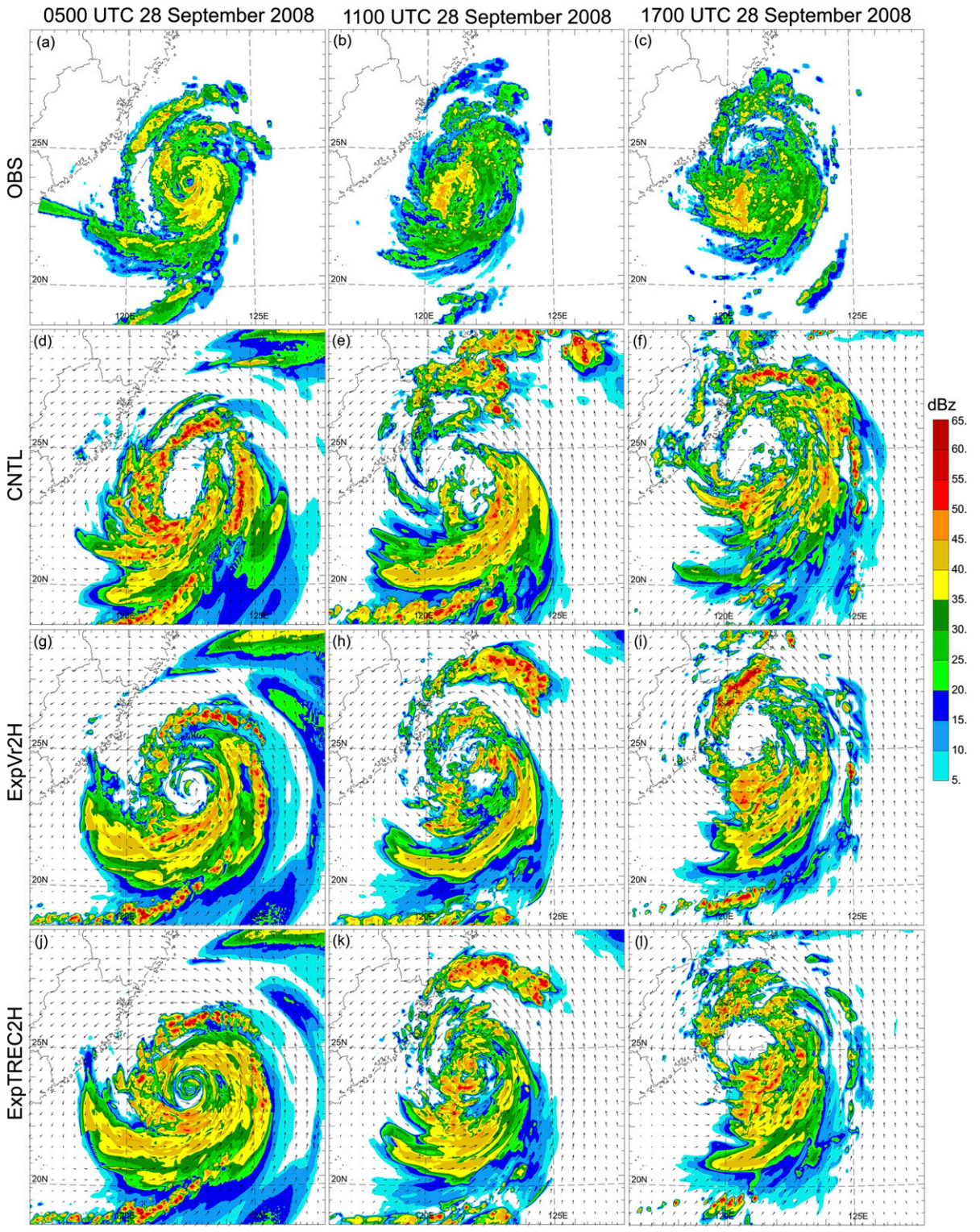

FIG. 6. Composite reflectivity (color shaded) and wind vectors at 3 km above the surface predicted by (d)–(f) CNTL, (g)–(i) ExpVr2H, and (j)–(l) ExpTREC2H, compared with (a)–(c) corresponding composite reflectivity observations at (from left to right) 0500, 1100, and 1700 UTC 28 Sep 2008.

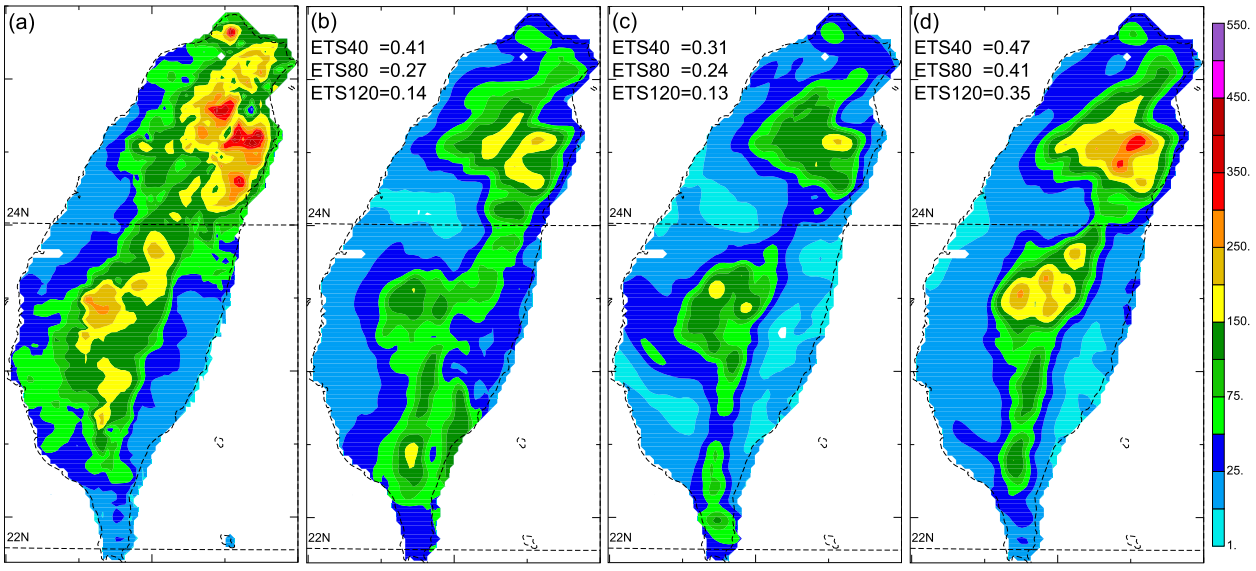

FIG. 7. 12-h accumulated precipitation from 0200 to 1400 UTC for (a) observations, (b) CNTL, (c) ExpVr2H, and (d) ExpTREC2H. The corresponding equitable threat scores for the thresholds of 40 mm (ETS40), 80 mm (ETS80), and 120 mm (ETS120) are shown in (b),(c), and (d), respectively.

data change? This question is examined through two experiments that are identical with ExpVr2H and ExpTREC2H except for the addition of *Z* data (Table 1).

a. Sensitivity to assimilation window length

Experiments ExpVr1H (ExpVr3H) and ExpTREC1H (ExpTREC3H) are the same as ExpVr2H and ExpTREC2H, respectively, except that the length of time during which DA is performed is changed to 1 (3) h. We can also consider ExpVr1H (ExpTREC1H) and ExpVr2H (ExpTREC2H) part of the longer DA experiment ExpVr3H (ExpTREC3H) with the difference being the time at which the forecast is launched. A summary and comparison of experiments is presented in Table 1.

Analyses and forecasts of MSLP and MSW during the assimilation cycles from 0000 to 0300 UTC are plotted in Fig. 8 to examine the direct impacts of data assimilation on typhoon intensity. ABT data and the CNTL forecast are also plotted for comparison. At the end of the 1-h

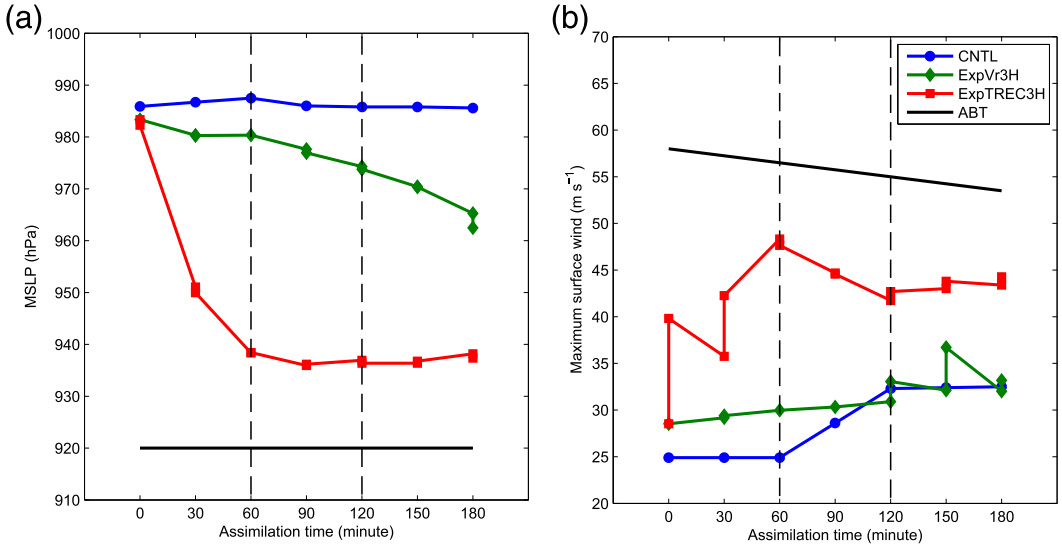

FIG. 8. Analysis and forecast (a) MSLP and (b) maximum surface winds during the analysis cycles from 0000 to 0300 UTC. The average best track data and the forecast of CNTL are plotted for comparison.

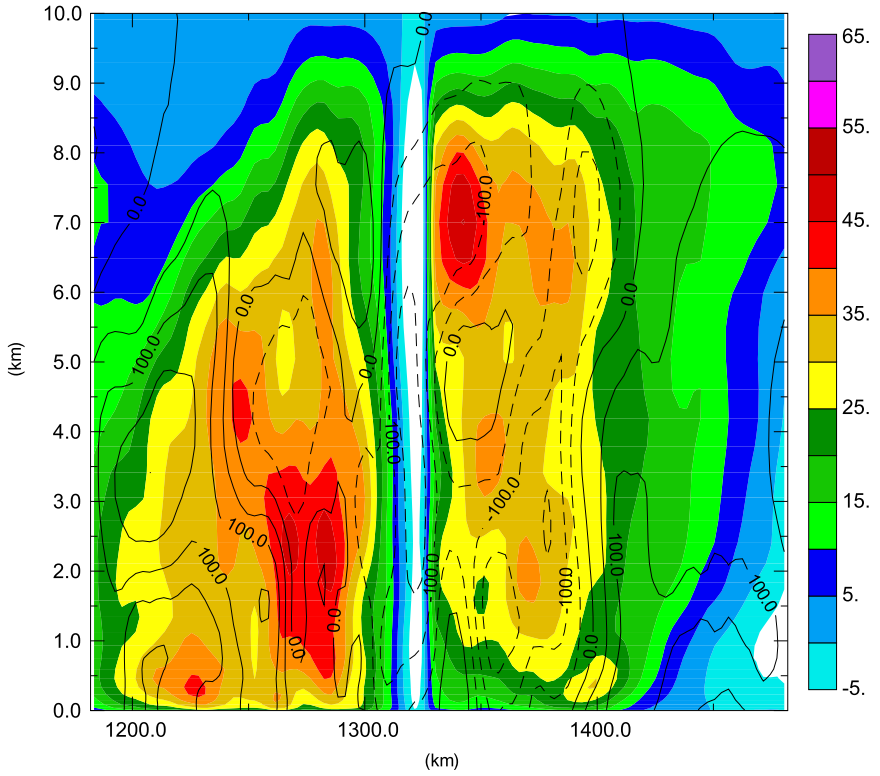

FIG. 9. Analysis increments of tangential wind (color shaded, m s^{-1}) and pressure (contours with 50 Pa interval) in the east–west vertical cross section through the analyzed typhoon center from ExpTREC2H, from the first analysis at 0000 UTC 28 Sep 2008.

assimilation window, the MSLP readings in ExpVr1H and ExpTREC1H decrease by 3 and 45 hPa, respectively; these values are 6 and 48 hPa lower than that of CNTL experiment, respectively. Over the next 2 h, when assimilating V_{TREC}, MSLP remains between 936 and 937 hPa, resulting in errors of 16–17 hPa against the ABT data. When assimilating V_r, the MSLP decreases from 980 to 962 hPa, resulting in an error of around 42 hPa compared to ABT data at the end of the DA period.

The MSW of ExpTREC2H (Fig. 8b) increases by about 11 m s^{-1} during the first EnKF analysis (time = 0 in the figure), while the MSW increment in ExpVr2H is very small. Assimilation of V_r only has a small impact on the MSW until later cycles, due to the limited number of near-surface inner-core observations of V_r early in the experiment. The MSW in the V_{TREC} assimilation experiments increases to about 48 m s^{-1} after 1 h of assimilation (60 min in the figure), 18 m s^{-1} higher than the MSW in the V_r assimilation experiments at the corresponding time. MSW later remains relatively steady in the V_{TREC} experiments, decreasing slightly to 43 m s^{-1} at 120 min, then increasing slightly to 45 m s^{-1} at 180 min. Throughout the 3 h, the MSW in the V_{TREC} experiments consistently remains approximately 10 m s^{-1} higher than the MSW in the V_r assimilation and CNTL experiments; the stronger analyzed surface vortex in the V_{TREC} experiments more closely matches the best track intensity.

Generally, as the number of assimilation cycles (and thus the length of assimilation window) increases, the differences in analyses produced using V_{TREC} and V_r assimilation becomes smaller, but even after 3 h of assimilation the analyzed vortex in ExpTREC3H remains much stronger than that of ExpVr3H, with MSLP and MSW differences between the experiments of 25 hPa and 10 m s^{-1}, respectively. Overall, assimilating V_{TREC} can effectively build up a strong typhoon vortex using a shorter data assimilation period; for real-time forecasting this would permit a longer forecast lead time prior to typhoon landfall. It takes much longer for V_r to establish the typhoon vortex, and the resultant vortex is weaker even after 3 h of DA.

We note from Fig. 8 that assimilation of V_{TREC} data is very effective in increasing the MSW, especially in the first analysis when the background vortex is too weak (Fig. 8b). In comparison, the reduction to the MSLP in the first as well as other cycles is minimal (Fig. 8a). To investigate how assimilation of V_{TREC} data impacts the wind and pressure fields, east–west vertical cross sections

of tangential wind and pressure analysis increments are plotted in Fig. 9 through the vortex center for the first analysis. Directly updated by the V_{TREC} data, the vortex circulation is greatly enhanced, with a maximum wind speed increment of over 45 m s^{-1}. EnKF analysis of V_{TREC} data reduces the pressure near the vortex center via cross-variable correlation between wind and pressure, but the maximum pressure reduction is only around 2 hPa. This rather small reduction is at least partly due to the relatively small ensemble spread in the near-surface pressure field. Compared to uncertainty in the wind forecast, which is relatively localized, the ensemble spread of pressure in the inner core of the TC is more related to the overall TC intensity uncertainty. All vortices in the background ensemble forecasts at 0600 UTC are too weak compared to observations, contributing to the underestimation of surface pressure ensemble spread.

The lowest altitude at which V_{TREC} data are available is 1 km; below this level, the tangential wind increment is achieved through spatial covariance subject to vertical covariance localization. Given that the vertical localization radius used is 4 km, localization reduction is relatively small at the surface. Still, spatial correlation tends to decrease with distance from the observations; as a result, the wind increment at the 1-km level is as large as 40 m s^{-1}, while the maximum wind increment at the surface is only around 25 m s^{-1}. The MSW after the first analysis is 11 m s^{-1} (Fig. 8b); this is because assimilation of V_{TREC} data also corrects the position of the strongest surface winds, reducing the radius of maximum wind in the vortex from about 100 km to about 40 km (not shown).

Most of the increase in MSW during DA is achieved in the analysis steps, while most of the MSLP reduction is achieved during the forecast steps (Fig. 8). Similar behavior was observed in Li et al. (2012), which used the WRF 3DVAR and WRF ensemble transform Kalman filter (ETKF)–En3DVar hybrid system to assimilate coastal radar radial velocity data for a landfalling hurricane. Almost all MSLP reductions in their experiments were also achieved during the forecast steps (see their Fig. 8b). The overall MSW increases and MSLP reductions are much more substantial when assimilating V_{TREC} data. The V_{TREC}-assimilating experiments create strong, closed circulations much more quickly than experiments assimilating V_r data (Figs. 8c and 4c). However, because the analysis step creates large wind increments but very small pressure increments, the balance of the analyzed wind and pressure fields may not be particularly good.

Within a typhoon vortex and above the boundary layer, the gradient wind balance is a reasonable approximation between the wind and pressure field. To examine

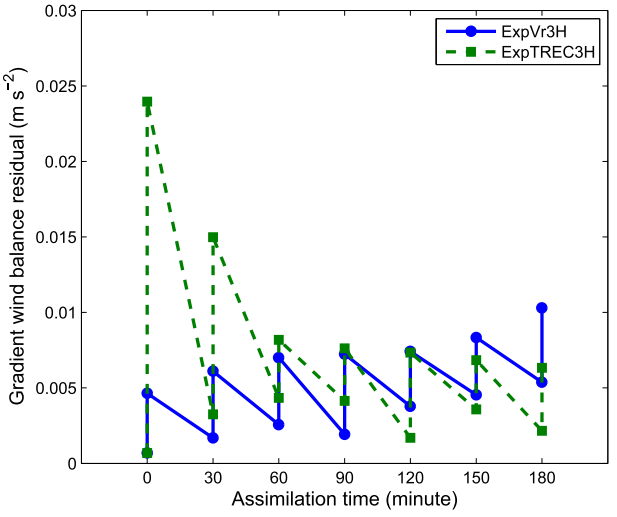

FIG. 10. The root-mean-square of the gradient wind balance residual for the analyses and forecasts from ExpVr3H and ExpTREC3H, during the analysis cycles from 0000 to 0300 UTC.

if and how the wind and pressure fields adjust to each other during the assimilation cycles, the gradient wind relation is diagnosed by calculating the residual of gradient wind balance (GWR), defined as

$$\mathrm{GWR} = \frac{V_T^2}{r} + fV_T - \frac{1}{\rho}\frac{\partial p}{\partial r},$$

where V_T is the tangential wind, p is the pressure, ρ is the air density, f is the Coriolis parameter, and r is the radius from vortex center. The root-mean-square (RMS) GWRs are calculated and plotted every kilometer from 0 to 12 km above the surface within a 300-km radius of the typhoon for analyses and forecasts during the DA period in Fig. 10. The calculation region is chosen to cover the main circulation of the typhoon; most of the direct impact of radar DA is confined to this region.

A higher value of RMS GWR means more wind–pressure imbalance, and vice versa. In general, the assimilation of V_{TREC} or V_r data induces imbalance between wind and pressure, but this imbalance is quickly reduced during the subsequent model forecast. The RMS GWR is increased from 0.001 to more than 0.02 m s^{-2} during the first analysis of V_{TREC} data (Fig. 10); this result is consistent with the significant increase in MSW with only a small reduction in MSLP noted in Fig. 8. After 30 min of forecast time, the RMS GWR is reduced to about 0.003 m s^{-2}, and after 1 h, the RMS GWRs in analyses and forecasts stabilize, remaining below 0.01 and 0.005 m s^{-2}, respectively, suggesting that the model pressure field in these later cycles has adjusted to match the vortex presented in the wind field. As a result, no large

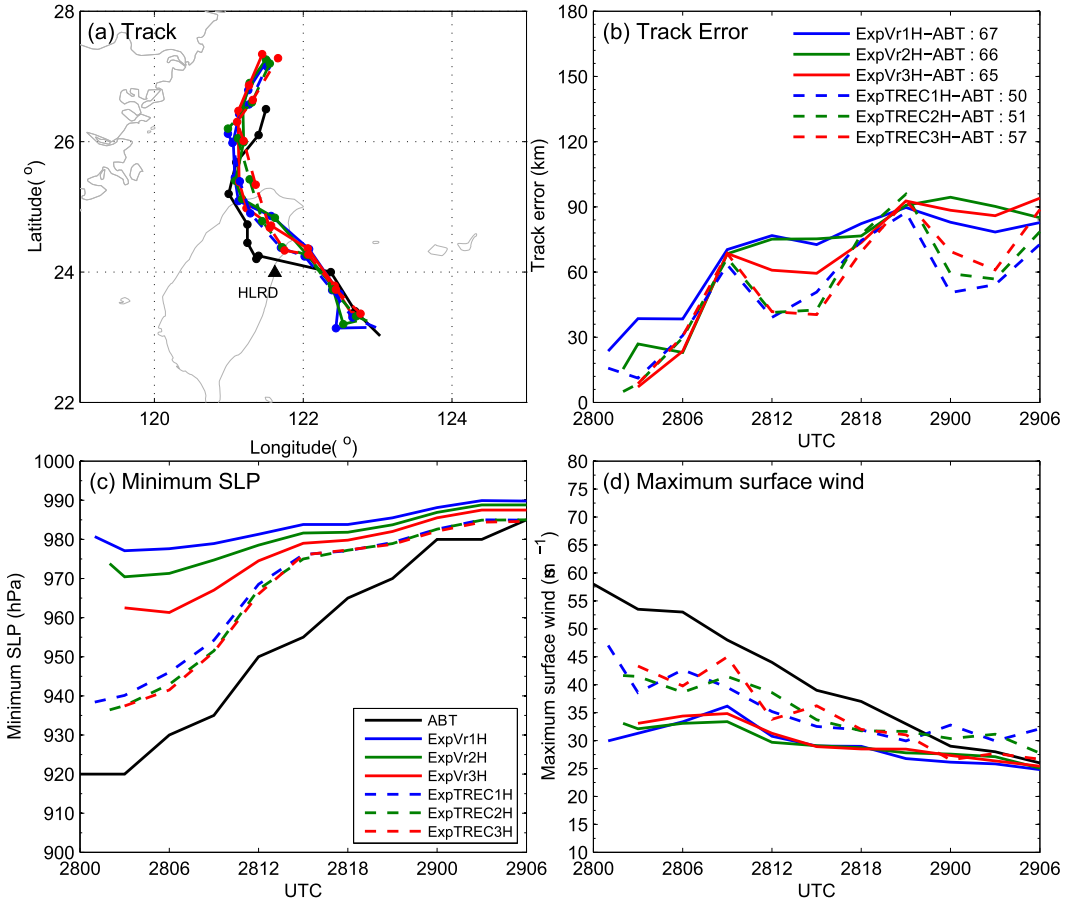

FIG. 11. The predicted (a) tracks, (b) track errors, (c) MSLPs, and (d) maximum surface wind speeds from 0100 (ExpVr1H, ExpTREC1H), 0200 (ExpVr2H, EpxTREC2H), and 0300 (ExpVr3H, ExpTREC3H) UTC 28 Sep to 0600 UTC 29 Sep 2008, along with the ABT (see section 2). The dots in (a) denote the center locations every 3 h starting from 0300 UTC 28 Sep. The ABT at 0100 and 0200 UTC 28 Sep is linearly interpolated from 0000 to 0300 UTC. The numbers in (b) denote the mean track errors over the 28-h forecast against the ABT.

discrepancy arises during the later cycles when the wind field is directly updated by the V_{TREC} assimilation, again demonstrating the ability of V_{TREC} assimilation to quickly build up a strong, balanced vortex through frequent DA cycles. In comparison, assimilation of V_r data creates less imbalance, due to much smaller wind increments. The RMS GWR increases slightly during assimilation in the V_r experiment, which may be due to the increased V_r data coverage, but remains below 0.01 and 0.005 m s^{-2} for the analyses and forecasts, respectively. This investigation indicates that even through the analyzed pressure and wind fields are not well balanced, especially when the wind increments are large, the pressure field can rather quickly adjust to the strengthened wind fields during the subsequent forecast step, especially when a strong vortex circulation is established in the analysis steps.

The predicted track, track error, MSLP, and MSW for ExpVr1H, ExpVr2H, ExpVr3H, ExpTREC1H, ExpTREC2H, and ExpTREC3H, respectively, are plotted in Fig. 11. For experiments assimilating V_r for varying lengths of time, the track forecasts show similar paths (Fig. 11a). The mean track errors are 67, 66, and 65 km in ExpVr1H, ExpVr2H, and ExpVr3H, respectively (Fig. 11b). The predicted tracks from ExpTREC1H, ExpTREC2H, and ExpTREC3H are similar, but their mean track errors of 50, 51, and 57 km, respectively, are smaller than those of the V_r–assimilating experiments (Figs. 11a,b). When assimilating V_r, due to the improved intensity analyses obtained when using a longer DA period, intensity forecasts are also improved, with mean MSLP errors of 26, 22, and 20 hPa in ExpVr1H, ExpVr2H, and ExpVr3H, respectively (Fig. 11c). In comparison, the MSLP forecasts from ExpTREC1H, ExpTREC2H, and ExpTREC3H are not sensitive to the assimilation window length; all have a much lower mean error of around 11 hPa. Consistent with the improved MSW analysis, the MSW forecasts from the V_{TREC} assimilation experiments agree

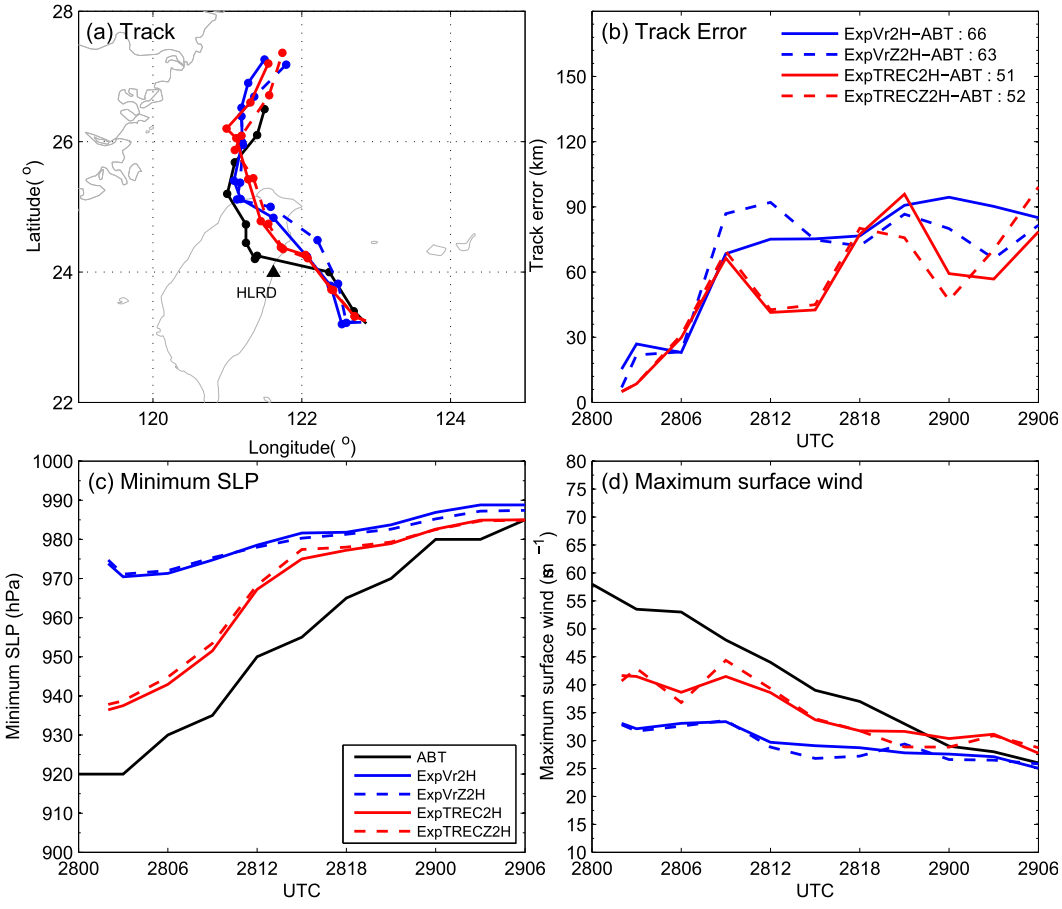

FIG. 12. The predicted (a) tracks, (b) track errors, (c) MSLPs, and (d) maximum surface wind speeds from 0200 UTC 28 Sep to 0600 UTC 29 Sep 2008 for ExpVr2H, ExpVrZ2H, ExpTREC2H, and ExpTRECZ2H, along with the ABT (see section 2). The dots in (a) denote the center locations every 3 h starting from 0300 UTC 28 Sep. The ABT at 0200 UTC 28 Sep is linearly interpolated from 0000 to 0300 UTC. The numbers in (b) denote the mean track errors over the 28-h forecast against the ABT.

better with observations than those of the experiments assimilating V_r data (Fig. 11d). The mean MSW errors from ExpTREC1H, ExpTREC2H, and ExpTREC3H are 6.9, 5.6, and 5.0 m s^{-1}, respectively, lower than those of ExpVr1H, ExpVr2H, and ExpVr3H, respectively. These results again show the advantage of assimilating V_{TREC} data as opposed to V_r data, particularly for shorter assimilation window lengths.

b. *Sensitivity to assimilation of reflectivity*

In ExpVrZ2H and ExpTRECZ2H, reflectivity data are assimilated alongside V_r or V_{TREC} from 0000 to 0200 UTC using EnKF (see Table 1) to investigate whether the relative impact of V_r and V_{TREC} is changed when Z data are included. Similar to DX13, our sensitivity experiments showed that using reflectivity to update the wind, potential temperature, and water vapor mixing ratio had a negative impact on the analysis (not shown). Therefore, reflectivity data are used to update only pressure and microphysical variables in our experiments. Compared to the assimilation of V_r or V_{TREC} in ExpVr2H and ExpTREC2H, the assimilation of additional Z data has little impact on the intensity analyses and forecasts (Fig. 12). The track forecasts of ExpVrZ2H and ExpTRECZ2H (Fig. 12a) are similar to those ExpVr2H and ExpTREC2H. The mean track errors are 63 and 52 km for ExpVrZ2H and ExpTRECZ2H, comparable to those of ExpVr2H and ExpTREC2H. The ETSs of 12-h accumulated precipitation are 0.34 and 0.49 for ExpVrZ2H and ExpTRECZ2H at the 40 mm threshold, and 0.13 and 0.32 at the 120 mm threshold, respectively; these values are similar to those obtained in ExpVr2H and ExpTREC2H (Fig. 7). Overall, assimilation of Z data does not substantively alter the relative impacts of V_r and V_{TREC} assimilation.

5. Conclusions and discussion

Radar reflectivity Z data have been used to retrieve winds using the recently developed TC circulation Tracking Radar Echo by Correlation (T-TREC) technique, which, in our implementation, also uses V_r observations to limit the correlation search region when available. This study examines, for the first time, the impacts of cycled assimilation of T-TREC retrieval winds (V_{TREC}) on TC analysis and forecasting using an EnKF. Typhoon Jangmi, which passed over Taiwan during September of 2008, is chosen as a test case. Radar data from a single coastal operational weather radar at Hualian, Taiwan, are assimilated prior to typhoon landfall.

The V_{TREC} or V_r data are assimilated at 30-min intervals during a 2-h window shortly after the typhoon entered the V_r coverage region of the Hualian operational radar. The assimilation of V_{TREC} data improves the intensity and structure of the typhoon significantly, while the assimilation of V_r data over the same time period yields a much smaller improvement due to limited V_r data coverage and poor retrieval of the cross-beam wind component. The improved analyses obtained by assimilating V_{TREC} data allows for better track, intensity, structure, and precipitation forecasts. Second, four sensitivity experiments using data assimilation periods of different lengths are performed. Results show that V_{TREC} assimilation can quickly (within 1 h) build up a strong vortex, while a longer period of cycled data assimilation is required when using V_r data to spin up the vortex. While the difference between V_{TREC} and V_r assimilation is smaller as the length of data assimilation increases, even after 3 h of data assimilation the analysis and forecasts obtained by assimilating V_{TREC} data are still much better than those obtained by assimilating V_r.

Assimilation of V_{TREC} (and, to a lesser extent, V_r) data effectively updates the wind fields and creates large wind increments in early data assimilation cycles, though the associated pressure increments are much smaller, resulting in an imbalance between the analyzed wind and pressure. Gradient wind balance diagnoses are performed to show that the pressure field can adjust quickly and efficiently to the enhanced wind fields, especially in the V_{TREC} assimilation experiments. As a result, MSLP reduction can be achieved during the forecast steps of the EnKF, since strong vortex circulations have already been established by the radar data assimilation.

Finally, when Z data are assimilated alongside V_r or V_{TREC} for 2 h in another pair of experiments, the relative impact of V_r and V_{TREC} assimilation is unchanged. Overall, because of more complete wind information (including the retrieved cross-beam component) and a larger spatial coverage of data, V_{TREC} assimilation is more effective than V_r assimilation, and can potentially provide good TC initialization and improved forecasts several hours earlier than V_r observations can as a TC approaches the coast. Although the conclusions here are based on a single landfalling typhoon case, the results obtained by assimilating V_{TREC} and V_r data for different lengths of time appears to be robust. More cases should be examined to confirm these conclusions in the future.

Compared to the single-time assimilation of V_{TREC} data for Typhoon Meranti (2010) in Li et al. (2013) using WRF 3DVAR, this study examines the impacts of cycled assimilation of V_{TREC} data using an EnKF on the analysis and forecast of the intense Typhoon Jangmi (2008). Consistent with Li et al. (2013), our results demonstrate the ability of V_{TREC} assimilation to quickly build up a strong vortex. In this study, the assimilation of V_{TREC} at the first analysis time also significantly improves the vortex circulation in the analysis, while subsequent cycles further improve the typhoon analysis and facilitate the establishment of a balanced vortex through wind-pressure adjustment.

A few other issues are worthy of future exploration. T-TREC-retrieved winds have a larger spatial coverage than GBVTD-retrieved winds, but may have less accuracy in the inner-core region of the TC for low-wavenumber components. Thus, it would be interesting to compare assimilation of T-TREC and GBVTD retrieval winds. The V_r data are not directly used for T-TREC wind retrieval; therefore, V_r is mostly independent of V_{TREC}. Thus, it may be possible to assimilate both V_r and V_{TREC} together to obtain better analyses than could be obtained assimilating V_{TREC} alone. It would also be interesting to compare the assimilation of V_{TREC} data and the assimilation of V_r data from multiple radars in a case where a typhoon is covered by multiple coastal radars. Understanding the relative impacts of assimilating individual data sources or their combinations using assimilation periods of varying length would also be valuable. These would be good topics for future studies.

Acknowledgments. This work was primarily supported by the Social Common Wealth Research Program (GYHY201006007), National Fundamental Research 973 Program of China (2013CB430100 and 2009CB421502), the National Natural Science Foundation of China (Grants 40975011 and 40921160381), and by the U.S. Office of Naval Research Grant DOD-ONR N00014-10-1-0775. Dr. Nathan Snook is thanked for his careful proofreading and editing of the manuscript.

REFERENCES

Anderson, R. J., 1993: A study of wind stress and heat flux over the open ocean by the inertial-dissipation method. *J. Phys. Oceanogr.,* **23,** 2153–2161.

Barker, D. M., W. Huang, Y. R. Guo, A. J. Bourgeois, and Q. N. Xiao, 2004: A Three-dimensional variational data assimilation system for MM5: Implementation and initial results. *Mon. Wea. Rev.,* **132,** 897–914.

Deardorff, J., 1980: Stratocumulus-capped mixed layers derived from a three-dimensional model. *Bound.-Layer Meteor.,* **18,** 495–527.

Dong, J., and M. Xue, 2013: Assimilation of radial velocity and reflectivity data from coastal WSR-88D radars using ensemble Kalman filter for the analysis and forecast of landfalling hurricane Ike (2008). *Quart. J. Roy. Meteor. Soc.,* **139,** 467–487.

Gourley, J. J., R. A. Maddox, K. W. Howard, and D. W. Burgess, 2002: An exploratory multisensor technique for quantitative estimation of stratiform rainfall. *J. Hydrometeor.,* **3,** 166–180.

Halverson, J. B., J. Simpson, G. Heymsfield, H. Pierce, T. Hock, and L. Ritchie, 2006: Warm core structure of Hurricane Erin diagnosed from high altitude dropsondes during CAMEX-4. *J. Atmos. Sci.,* **63,** 309–324.

Hamill, T. M., J. S. Whitaker, M. Fiorino, and S. G. Benjamin, 2011: Global ensemble predictions of 2009's tropical cyclones initialized with an ensemble Kalman filter. *Mon. Wea. Rev.,* **139,** 668–688.

Harasti, P. R., C. J. McAdie, P. P. Dodge, W.-C. Lee, J. Tuttle, S. T. Murillo, and F. D. Marks, 2004: Real-time implementation of single-Doppler radar analysis methods for tropical cyclones: Algorithm improvements and use with WSR-88D display data. *Wea. Forecasting,* **19,** 219–239.

Landsea, C. W., and J. L. Franklin, 2013: Atlantic hurricane database uncertainty and presentation of a new database format. *Mon. Wea. Rev.,* **141,** 3576–3592.

Li, X., J. Ming, Y. Wang, K. Zhao, and M. Xue, 2013: Assimilation of T-TREC-retrieved wind data with WRF 3DVAR for the short-term forecasting of Typhoon Meranti (2010) near landfall. *J. Geophys. Res. Atmos.,* **118,** 10 361–10 375, doi:10.1002/jgrd.50815.

Li, Y., X. Wang, and M. Xue, 2012: Assimilation of radar radial velocity data with the WRF hybrid ensemble–3DVAR system for the prediction of Hurricane Ike (2008). *Mon. Wea. Rev.,* **140,** 3507–3524.

Lin, Y.-L., R. D. Farley, and H. D. Orville, 1983: Bulk parameterization of the snow field in a cloud model. *J. Climate Appl. Meteor.,* **22,** 1065–1092.

Liu, Y., D.-L. Zhang, and M. K. Yau, 1999: A multiscale numerical study of Hurricane Andrew (1992). Part II: Kinematics and inner-core structures. *Mon. Wea. Rev.,* **127,** 2597–2616.

Makin, V. K., 2005: A note on the drag of the sea surface at hurricane winds. *Bound.-Layer Meteor.,* **115,** 169–176.

Powell, M. D., P. J. Vickery, and T. A. Reinhold, 2003: Reduced drag coefficient for high wind speeds in tropical cyclones. *Nature,* **422,** 279–283.

Ren, D., and M. Xue, 2004: A revised force–restore model for land surface modeling. *J. Appl. Meteor.,* **43,** 1768–1782.

Stern, D. P., and D. S. Nolan, 2012: On the height of the warm core in tropical cyclones. *J. Atmos. Sci.,* **69,** 1657–1680.

Torn, R. D., 2010: Performance of a mesoscale ensemble Kalman filter (EnKF) during the NOAA high-resolution hurricane test. *Mon. Wea. Rev.,* **138,** 4375–4392.

——, and C. Snyder, 2012: Uncertainty of tropical cyclone best-track information. *Wea. Forecasting,* **27,** 715–729.

Tuttle, J., and R. Gall, 1999: A single-radar technique for estimating the winds in tropical cyclones. *Bull. Amer. Meteor. Soc.,* **80,** 653–668.

Wang, M. J., K. Zhao, and D. Wu, 2011: The T-TREC technique for retrieving the winds of landfalling typhoons in China. *Acta Meteor. Sin.,* **25,** 91–103.

Whitaker, J. S., and T. M. Hamill, 2012: Evaluating methods to account for system errors in ensemble data assimilation. *Mon. Wea. Rev.,* **140,** 3078–3089.

Xiao, Q., Y.-H. Kuo, J. Sun, W.-C. Lee, E. Lim, Y.-R. Guo, and D. M. Barker, 2005: Assimilation of Doppler radar observations with a regional 3DVAR system: Impact of Doppler velocities on forecasts of a heavy rainfall case. *J. Appl. Meteor.,* **44,** 768–788.

——, ——, ——, ——, D. M. Barker, and E. Lim, 2007: An approach of radar reflectivity data assimilation and its assessment with the inland QPF of Typhoon Rusa (2002) at landfall. *J. Appl. Meteor. Climatol.,* **46,** 14–22.

Xue, M., and J. Dong, 2013: Assimilating best track minimum sea level pressure data together with Doppler radar data using an ensemble Kalman filter for Hurricane Ike (2008) at a cloud-resolving resolution. *Acta Meteor. Sin.,* **27,** 379–399, doi:10.1007/s13351-013-0304-7.

——, K. K. Droegemeier, V. Wong, A. Shapiro, and K. Brewster, 1995: ARPS version 4.0 user's guide. University of Oklahoma, 380 pp. [Available online at http://www.caps.ou.edu/ARPS.]

——, J. Zong, and K. K. Droegemeier, 1996: Parameterization of PBL turbulence in a multi-scale non-hydrostatic model. Preprints, *11th Conf. on Numerical Weather Prediction,* Norfolk, VA, Amer. Meteor. Soc., 363–365.

——, K. K. Droegemeier, and V. Wong, 2000: The Advanced Regional Prediction System (ARPS)—A multi-scale nonhydrostatic atmospheric simulation and prediction model. Part I: Model dynamics and verification. *Meteor. Atmos. Phys.,* **75,** 161–193.

——, and Coauthors, 2001: The Advanced Regional Prediction System (ARPS)—A multi-scale nonhydrostatic atmospheric simulation and prediction tool. Part II: Model physics and applications. *Meteor. Atmos. Phys.,* **76,** 143–165.

Zhang, F., Y. Weng, J. A. Sippel, Z. Meng, and C. H. Bishop, 2009: Cloud-resolving hurricane initialization and prediction through assimilation of Doppler radar observations with an ensemble Kalman filter. *Mon. Wea. Rev.,* **137,** 2105–2125.

Zhao, K., and M. Xue, 2009: Assimilation of coastal Doppler radar data with the ARPS 3DVAR and cloud analysis for the prediction of Hurricane Ike (2008). *Geophys. Res. Lett.,* **36,** L12803, doi:10.1029/2009GL038658.

——, ——, and W. C. Lee, 2012a: Assimilation of GBVTD-retrieved winds from single-Doppler radar for short-term forecasting of Super Typhoon Saomai (0608) at landfall. *Quart. J. Roy. Meteor. Soc.,* **138,** 1055–1071.

——, X. F. Li, M. Xue, B. J. D. Jou, and W. C. Lee, 2012b: Short-term forecasting through intermittent assimilation of data from Taiwan and mainland China coastal radars for Typhoon Meranti (2010) at landfall. *J. Geophys. Res.,* **117,** D06108, doi:10.1029/2011JD017109.

Zhao, Q., and Y. Jin, 2008: High-resolution radar data assimilation for Hurricane Isabel (2003) at landfall. *Bull. Amer. Meteor. Soc.,* **89,** 1355–1372.